Carbohydrate Polymers 323 (2024) 121454

Contents lists available at ScienceDirect

Carbohydrate Polymers

journal homepage: www.elsevier.com/locate/carbpol

Impact of coagulation solvent interactions on porous morphology evolution in cellulose xerogels

Ashlee Aiello *, Huong Giang Nguyen, Christopher M. Stafford, Jeremiah W. Woodcock *

National Institute of Standards and Technology, 100 Bureau Drive, Gaithersburg, MD 20899, USA

ARTICLE INFO

Keywords:
Xerogel
Mesoporous
Cellulose
Biopolymer
Ionic liquid
[EMIm][OAc]

ABSTRACT

The role of coagulation solvent interactions on the pore formation mechanism in cellulose xerogels was investigated using single-step coagulation baths. A series of cellulose xerogels were fabricated from cotton yarns partially dissolved in ionic liquid (i.e., 1-ethyl-3-methylimidazolium acetate) and then immersed in one of seven different coagulation baths. These samples were evaluated using N_2 physisorption, inverse gas chromatography, and X-ray photoelectron spectroscopy. The regenerated cellulose orientation and resultant surface hydrophilicity was found to be dependent on solvent solubility interactions with an emphasis on polar interaction and dispersion force strength. More importantly, the xerogel specific surface area dramatically decreased from 100 m^2g^{-1} to 0.278 m^2g^{-1} with increasing hydrophilicity, confirming the importance of controlled cellulose orientation during the coagulation step of cellulose xerogel fabrication. These results have been used to propose a new pore formation mechanism in cellulose xerogels and provide recommendations towards the development of controllable porosity during xerogel fabrication.

1. Introduction

Plant-based cellulose is highly abundant, biodegradable, and biocompatible with high tensile strength (287 MPa to 800 MPa) and elastic modulus (5.5 GPa to 12.6 GPa) (Ramamoorthy, Skrifvars, & Persson, 2015). These desirable material properties have established cellulose as a primary raw material in multiple industries including textiles, pharmaceuticals, infrastructure materials, polymer composites, and food. The strong hydrogen bonding network, high variability in composition and structure, and hygroscopic nature of plant-based cellulose has historically presented processing challenges that restricted the development of new applications for this sustainable material. Cellulose cannot be melted, and typical solvents for dissolution such as carbon disulfide, aqueous metal salt solutions, and *n*-methylmorpholine n-oxide monohydrate as well as more recently reported solutions capable of cellulose dissolution (e.g., molten salt hydrates, aqueous NaOH solutions, and ammonia or ethylenediamine mixtures with thiocyanate salts) present disadvantages such as high cost, volatility, or high toxicity (Gericke, Schlufter, Liebert, Heinze, & Budtova, 2009). New advanced functionalization methods as well as the identification of new dissolution media such as ionic liquids (ILs) have helped to address these issues. ILs also present the added advantage of a less aggressive dissolution approach that solubilizes cellulose while leaving the alcohol groups intact, unlike other solvents. One emerging technology that makes use of these developments is the formation of cellulose xerogels, which are high surface area, low density, mesoporous (pore diameter = 2 nm to 50 nm) materials.

Cellulose xerogels are produced using a facile three-step processing method—(1) cellulose dissolution (e.g., IL treatment), (2) immersion into a coagulation bath (i.e., simultaneous removal of IL and regeneration of the dissolved cellulose), and (3) ambient drying. This process helps preserve the self-assembled porous network by eliminating pore-damaging freeze-drying or water-induced hornification effects that occur during aerogel fabrication, especially from aqueous solutions (Jin, Nishiyama, Wada, & Kuga, 2004). Xerogels are also more likely to promote uniformity in the porous network over aero- or cryogels produced by freeze-drying or supercritical CO_2 drying, respectively, by eliminating water swelling effects including swelling rate changes between different cellulose phases (e.g., amorphous cellulose versus cellulose Iβ) that can result in ballooning (Budtova & Navard, 2015). The xerogel can be produced in single phase or biphasic (i.e., regenerated xerogel phase surrounding an undissolved non-porous core) depending on whether the cellulose is fully or partially dissolved during the dissolution step. While biphasic cellulose xerogels with high specific

* Corresponding authors.
E-mail addresses: ashlee.aiello@nist.gov (A. Aiello), jeremiah.woodcock@nist.gov (J.W. Woodcock).

https://doi.org/10.1016/j.carbpol.2023.121454
Received 11 September 2023; Received in revised form 29 September 2023; Accepted 30 September 2023
Available online 5 October 2023
0144-8617/Published by Elsevier Ltd.

surface area (149 m^2g^{-1}) and porosity (0.5) have been successfully fabricated (Aiello, Cosby, McFarland, Durkin, & Trulove, 2022), identification of the pore morphology mechanism is required for industrial application development. Previous studies (Aiello, Cosby, Durkin, & Trulove, 2022; Aiello, Cosby, McFarland, et al., 2022) have presented a potential mechanism, influenced by the research of Lindman et al. on the role of amphiphilicity on cellulose dissolution (Alves et al., 2015; Lindman, Karlström, & Stigsson, 2010; Medronho et al., 2015; Medronho & Lindman, 2014; Medronho & Lindman, 2015; Medronho, Romano, Miguel, Stigsson, & Lindman, 2012), where the coagulation solvent polarity may lead to preferential interactions with the amphiphilic cellulose chains to form a mesoporous matrix. While this is supported by morphology studies of regenerated cellulose from ionic liquid solution in the literature (Geng & Henderson, 2014; Östlund, Idström, Olsson, Larsson, & Nordstierna, 2013), testing of this hypothesis has proven especially challenging, due to the complexity of interactions between the IL, dissolved cellulose, and coagulation solvent. Porous cellulose materials using aqueous or traditional solvents is generally limited to aero- or cryogel fabrication (Buchtová & Budtova, 2016; Budtova, 2019; Budtova & Navard, 2015), although some xerogels have been produced from functionalized cellulose or through the use of multiple solvent rinses to overcome hornification effects (Yamasaki et al., 2019). Xerogels have also been synthesized using emulsion templating using interfacial oil and cellulose solution layers (Ganesan, Dennstedt, Barowski, & Ratke, 2016).

We hypothesized that pore formation in cellulose xerogels is influenced by coagulation solvent interactions. This study examines the role of the coagulation solvent during cellulose regeneration to elucidate the pore formation mechanism in cellulose xerogels in order to control the porous morphology evolution. Both the normalized Reichardt's polarity parameter, E_T^N, (Reichardt, 1994, 2005) and Hansen solubility parameters (dispersion force, polar interaction, and hydrogen bonding force) were used to assess the different aspects of solvent behavior on material properties in cellulose xerogels. Although E_T^N is among the most commonly used parameters to compare solvatochromic data, it is dependent on both polarity (but not polarizability) and acidity (i.e., hydrogen bond donating ability) (Jessop, Jessop, Fu, & Phan, 2012). The Hansen solubility parameters allow for a clearer, less convoluted assessment of the different interactions governing solvent interactions and are more commonly used to assess polymers.

A series of cellulose xerogels were fabricated using a single solvent coagulation bath from cotton yarn. Commercially available cotton yarn was used to more closely replicate industry-relevant conditions, including potential circular economy applications such as cellulose xerogel fabrication from recycled cotton fabrics. Seven different coagulation solvents with varying solvation behavior were used to fabricate the sample series. The normalized Reichardt's polarity parameter, E_T^N, and Hansen solubility parameters of each solvent were compared to examine the impact of solvation behavior on specific surface area, surface energy, and hydrophilicity measured using nitrogen gas physisorption and inverse gas chromatography (iGC). These measurements confirmed that decreasing coagulation solvent polarity produces a more hydrophobic surface, although this effect becomes limited in low polarity solvents. This was attributed to decreased IL solubility that we hypothesize results in slowed cellulose regeneration kinetics to produce a more favored thermodynamic architecture. We go on to discuss these findings, including how controlled porosity may be achieved, and propose a new pore formation mechanism.

2. Methods

2.1. General

Equipment and materials are identified in the article to adequately specify the experimental details. Such identification does not imply recommendation by the National Institute of Standards and Technology, nor does it imply that the materials are necessarily the best available for the purpose.

2.2. Materials

Methanol (MeOH, ≥99.8 %, Fisher Chemical), ethanol (EtOH, ≥99.5 %, Warner Graham Company), isopropyl alcohol (IPA, ≥99.5 %, Fisher Chemical), 1-propanol (PrOH, ≥99.0 %, Macron Fine Chemicals), 1-butanol (1-B, ≥99.4 %, Taylor Chemical Company), acetonitrile (ACN, ≥99.9 %, J.T. Baker), n,*n*-dimethylformamide (DMF, ≥99.8 %, Sigma Aldrich), 1-ethyl-3-methylimidazolium acetate ($[C_2C_1Im][OAc]$, ≥95.0 %, Io-Li-Tec), and commercially available cotton thread (Coats & Clark Machine Quilting Cotton Thread) were used as-received. $[C_2C_1Im][OAc]$ was stored in an Ar drybox environment upon receiving to minimize water contamination.

2.3. Sample fabrication

Cotton thread (≈ 0.5 g) was hand-wound around polytetrafluoroethylene jigs under minimal tension with no interlapping of adjacent yarns (Fig. S1). Loaded jigs were dried at 60 °C under atmospheric pressure overnight to reduce the impact of residual water from the cotton thread by maintaining a consistent environment prior to IL treatment. IL treatments were performed in Ar drybox environment to minimize water contamination caused by the hygroscopic nature of the cotton threads and IL. Ten minutes prior to IL treatment, jigs were transferred into Ar drybox environment and placed on the hot plate used for preheating the IL to minimize temperature gradient effects. The heated loaded jigs were then placed in IL at 60 °C for 30 min, then submerged in coagulation solvent. The 30 min treatment time was chosen based on previously reported data showing that this time was sufficient to maximize specific surface area without requiring additional dissolution time (Aiello, Cosby, Durkin, & Trulove, 2022). Note that this results in a biphasic cotton yarn morphology where ≈ 0.65 volume fraction of the yarn is formed of regenerated cellulose surrounding an undissolved cellulose core (≈ 0.35 volume fraction of the yarn) (Aiello, Cosby, Durkin, & Trulove, 2022). The submerged yarns were removed from the drybox, then loaded in a Soxhlet extractor within 5 to 10 min for continued coagulation using clean, heated coagulation solvent for 7 d. Seven different coagulation solvents were used—MeOH, EtOH, IPA, PrOH, 1-B, ACN, and DMF. Coagulated samples were then removed from the Soxhlet extractor and dried at 60 °C overnight with the exception of the sample fabricated using DMF, which was dried under vacuum due to the high boiling point of DMF.

An as-received cotton yarn reference sample was washed with an acetone Soxhlet rinse for 2 d, then dried in at 60 °C to obtain an accurate measurement of the as-received cotton yarn surface in the absence of any contamination or commercial surface coatings.

2.4. Characterization

2.4.1. N_2 Physisorption

Specific surface area and pore size distribution were determined from N_2 physisorption isotherms at 77 K up to ≈ 100 kPa (1 bar) measured on the analysis ports of a low-pressure manometric instrument (Autosorb iQ MP, Quantachrome Instruments, Boynton Beach, FL (now a subsidiary of Anton Paar)). Prior to each isotherm measurement, samples (≈ 0.5 g to 0.7 g) were outgassed under high vacuum at 105 °C for 48 h followed by cooling to room temperature and backfilling with nitrogen. The Brunauer-Emmett-Teller (BET) specific surface area was calculated using the partial pressure region $0.05 \leq P/P_0 \leq 0.3$ of the adsorption isotherms. The pore size distribution was determined using the Barret-Joyner-Halenda (BJH) method from the adsorption isotherm within the partial pressure range $0.35 \leq P/P_0 \leq 0.95$. Full nitrogen isotherms are not reported for as-received cotton and samples prepared

from the MeOH coagulation bath due to their low surface area. The estimated measurement uncertainty was determined from the relative standard deviation of measurements on a NIST zeolite reference material, which was 3 %.

2.4.2. iGC

Surface properties were measured using iGC (iGC-Surface Energy Analyzer, Surface Measurement Systems). An initial pretreatment step was used to dry samples (≈ 0.5 m^2 using the measured BET surface area from N_2 physisorption) under 10 sccm air flow at 100 °C and 0 % relative humidity for 3 h. Dead volume was measured using methane injection prior to the first step and after the last step. N-alkane (nonane, octane, heptane, and hexane) and polar (ethyl acetate, dicholormethane, ethanol, acetone, and acetonitrile) analyte probes were measured for a target fractional surface coverage range of 0.01–0.45 using 30 °C column temperature, 0 % relative humidity, and 10 sccm gas flow. Ethyl acetate and dicholormethane were selected as the acidic and basic probes, respectively, for specific surface area measurements. The estimated measurement uncertainty was determined from the average relative standard deviation of the retention volume for the solvent probes from three measurements, which was 0.53 %.

2.4.3. X-ray photoelectron spectroscopy (XPS)

IL removal and surface elemental analysis of the fabricated samples was confirmed by XPS (AXIS Ultra DLD Spectrometer, Kratos Analytical). XPS measurements were performed using a monochromatic Al K_α source (1486.6 eV) operating at 140 W. The base pressure of the sample analysis chamber was ≈1.33×10^7 Pa (or 1.0×10^9 Torr), and spectra were collected from a nominal spot size of 300 μm × 700 μm. Measurements were performed in hybrid mode using electrostatic and magnetic lenses, and the pass energy of the analyzer was set at 160 eV for survey scans with an energy resolution of 0.5 eV. Three measurements were taken for each sample. All XPS data analysis was completed using the CasaXPS software package.

3. Results

Coagulation solvents ranging in solvent polarity (using the normalized Reichardt's polarity parameter, E_T^N) were chosen on the basis that they formed a solution with neat [C_2C_1Im][OAc] (Table S1). The resultant solvents have a polarity range of $0.40 \leq E_T^N \leq 0.76$ with DMF being the most non-polar coagulation solvent ($E_T^N = 0.40$) and MeOH being the most polar coagulation solvent ($E_T^N = 0.76$) (Bosch & Roses, 1992; Dutkiewicz, 1990; Jessop et al., 2012). XPS measurements confirmed the removal of the nitrogen-containing IL from the fabricated samples using the measured nitrogen concentration (Table S2). More specifically, nitrogen concentrations were lower in fabricated samples compared with the as-received cotton yarn, the exception being samples fabricated with an ACN coagulation bath which showed a 0.29 % increase in the relative atomic concentration of nitrogen. Calcium and silicon were measured in the as-received cotton yarns, which is attributed to commercial coating residue that was not completely removed by the acetone Soxhlet wash. Calcium was not detected in the fabricated sample surfaces, and silicon levels were decreased by several % in the relative atomic concentration, indicating full removal of the commercial coating. In the case of samples rinsed using a 1-B coagulation bath, 1.49 % relative atomic concentration of fluorine was measured. This is likely a contaminant from our fabrication process.

N_2 physisorption isotherms of the fabricated samples and pore size distribution are shown in Fig. 1. As-received cotton yarn and samples coagulated with MeOH, ACN, and DMF were non-porous with low specific surface area. Note that full N_2 isotherms of as-received cotton and samples rinsed with MeOH are not reported due to their low specific surface area. The remaining samples (IPA, EtOH, PrOH, and 1-B) were mesoporous (i.e., 2 nm to 50 nm diameter pore size) as shown by their Type IV isotherms and average pore diameters of 5.6 nm to 7.8 nm (Al-Ghouti & Da'ana, 2020; Sing, Everett, Rierotti, Rouquerol, & Siemieniewska, 1985). These Type IV samples showed Type H2 hysteresis loops (EtOH, PrOH) indicative of uniform pore size and shape or Type H4 hysteresis loops (IPA, 1-B) characteristic of narrow slit-like pores from IUPAC classification guidelines (Sing et al., 1985; Sing & Williams, 2004). The highest surface area sample, coagulated from IPA, shows a peak at 5.6 nm with an additional hump at ≈ 4.9 nm (Fig. 1b). The presence of a secondary peak at a smaller pore size (≈ 4.9 nm) combined with increased N_2 uptake in the low P/P_0 ($\leq$ 0.1 P/P_0) region of the N_2 adsorption isotherm suggests this sample contains smaller pores compared with the other measured samples and may contain some micropores (pore diameter < 2 nm) that cannot be measured using the BJH method. As the specific surface area decreases, the average pore size increases from 5.6 nm to 7.8 nm (1-B), and the pore size distribution widens and shifts towards larger pore diameters.

iGC was chosen as a preferred method for surface energy measurements due to its independence of surface roughness, which provides a more accurate measurement over more traditional contact angle mea-

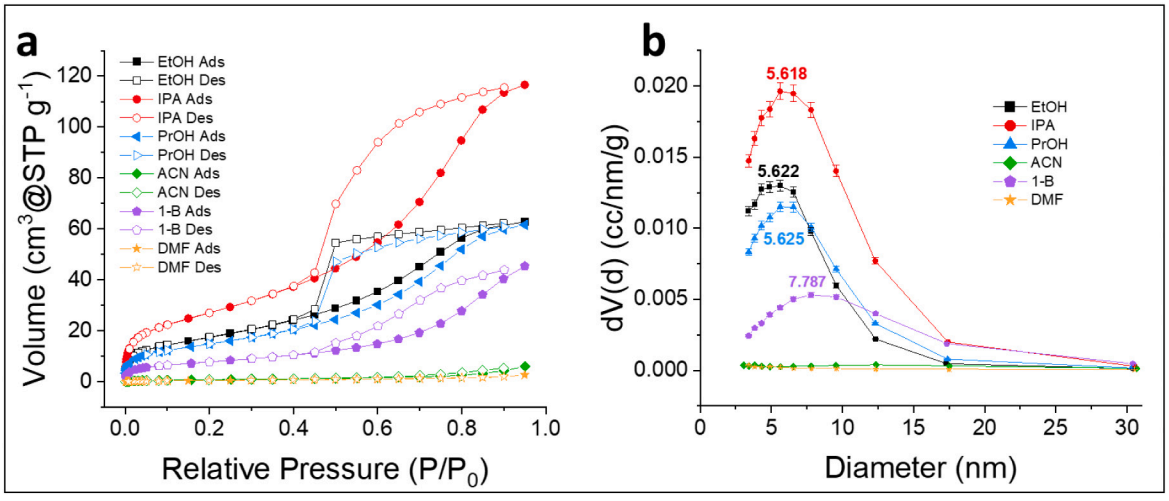

Fig. 1. N_2 physisorption (a) isotherms and (b) adsorption BJH pore size distribution of samples fabricated with different coagulation solvents. The average BJH pore sizes of porous samples are labeled in (b). The average BJH pore sizes of porous samples are labeled in (b) where error bars represent the estimated measurement uncertainty. The legends are listed in order of decreasing solvent polarity using the normalized Reichardt's polarity parameter. As-received cotton and samples fabricated using a MeOH coagulation bath are not reported due to their low surface area.

surements for mesoporous materials by measuring the retention time of individual gas probes as they interact with a surface. Heterogeneous iGC, or iGC measurements over a range of surface coverages, of the fabricated and as-received cotton yarns measured dispersive surface energy (γ_s^D), specific surface energy (γ_s^{SP}), Lewis acid constant (K_a), and Lewis base constant (K_b) for sample surface coverages ranging from 5 % to 20 % (Fig. 2). Although measurements were taken for estimated surface coverages ranging from 1 % to 45 %, the higher surface area samples tended to produce more variation in the actual surface coverage, especially for high surface coverages. This is attributed to a combination of changes in interaction strength between the various analyte probes and the sample surfaces as well as capillary effects of the adsorbed analyte probe within the mesoporous matrix. Since γ_s^{SP} is limited to polar molecular interactions while γ_s^D results from London forces, the measured surface energies could then be used to determine the hydrophilicity of the surface (γ_S^{SP}/γ_S^T) shown in Fig. 3, where γ_S^T is the total surface energy, or the sum of the dispersive and specific surface energies (Mohammadi-Jam & Waters, 2014). While the as-received cotton yarns were heterogenous for each of these properties (i.e., the measured value for a given surface property changes with respect to surface coverage), the regenerated cellulose samples were comparatively homogenous (i.e., constant measured value as a function of surface coverage) with lower dispersive surface energy, specific surface energy, Lewis acid constant, Lewis base constant, and hydrophilicity for nearly all surface coverages and coagulation solvents.

Fig. 4 provides a clearer comparison of the role of the coagulation solvent by limiting the scope of analysis to a single surface coverage (5 %) to elucidate more specific trends among the sample series. This coverage was selected due to the general homogeneity of the samples and the reduced variability in measured surface coverage for lower surface coverages. The measurements are organized in order of decreasing solvent polarity using E_T^N. When focusing on the regenerated cellulose samples, no clear trend is observable in the specific surface energy or Lewis base constant with respect to the solvent polarity. The dispersive surface energy reaches a maximum while minimum values are measured for the Lewis acid constant and hydrophilicity at mid-range solvent polarities (i.e., IPA, PrOH). As the solvent polarity continues to decrease ($E_T^N < 0.5$), the surface properties of the regenerated cellulose return to values similar to those measured for more polar solvents ($E_T^N > 0.65$).

Solvation is governed by intermolecular forces between the molecules of interest, which can be separated into three primary components—dispersion forces, polar interactions, and hydrogen bonding forces. The Hansen solubility parameters (dispersion forces ($\delta_{disperse}$), polar interactions (δ_{polar}), and hydrogen bonding forces ($\delta_{h\text{-}bonding}$)) provide a means to compare the strength of these components in different molecules. These parameters can be measured by iGC using various combinations of gas probe molecules with well-defined cross-sectional area and polarity (i.e., n-alkane probes for $\delta_{disperse}$, polar probes for δ_{polar}, and alcohol and n-alkane probes for $\delta_{h\text{-}bonding}$) (Gamelas, 2013; Mohammadi-Jam & Waters, 2014). Similar relationships exist for the measured surface properties where n-alkane probes are used to measure γ_S^D, acid and base probes to measure γ_S^{SP}, and polar and n-alkane probes to measure K_a and K_b. We have differentiated between protic and aprotic solvent types in our comparisons since the hydrogen bonding capability of protic solvents is likely to impact interactions with dissolved cellulose and the IL. Fig. 5 compares the γ_S^D and γ_S^{SP} measured at 5 % surface coverage with the Hansen solubility parameters of each solvent. γ_S^D increased with increasing $\delta_{disperse}$ and decreased with increasing δ_{polar} while γ_S^{SP} decreased with increasing $\delta_{disperse}$ and increased with increasing δ_{polar}. However, additional solvents must be tested to more accurately confirm these relationships. The data relating to hydrogen bonding showed strong scattering with no observable correlation.

Fig. 6 shows the relationship between hydrophilicity and the Hansen solubility parameters. The data suggests that the Hansen solubility parameters play a stronger role in surface hydrophilicity compared with γ_S^D and γ_S^{SP}. The hydrophilicity increased with increasing polar interaction strength and decreased with increasing dispersion force strength with

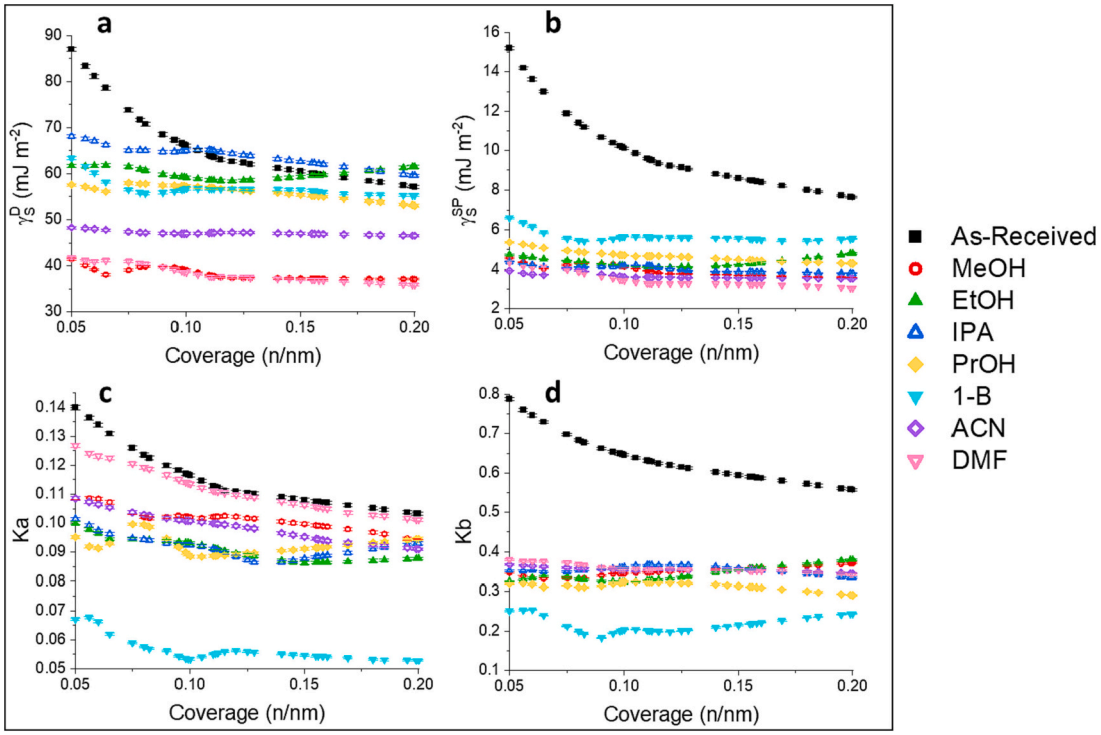

Fig. 2. Heterogeneous iGC of regenerated cellulose fabricated using different coagulation solvents. Measured surface properties are (a) dispersive surface energy, (b) specific surface energy, (c) Lewis acid constant (K_a), and (d) Lewis base constant (K_b). The legend is listed in order of decreasing solvent polarity using the normalized Reichardt's polarity parameter.

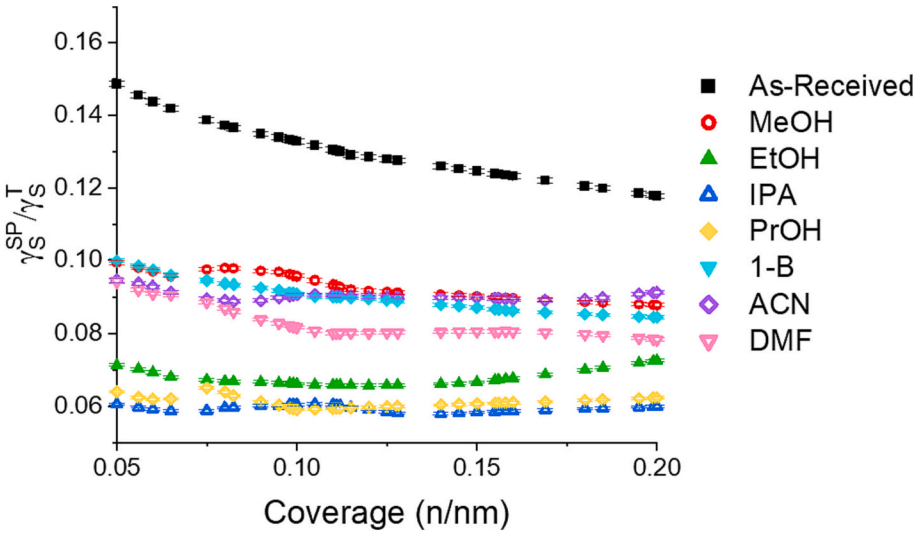

Fig. 3. Heterogeneous hydrophilicity of regenerated cellulose fabricated using different coagulation solvents measured using iGC. The legend is listed in order of decreasing solvent polarity using the normalized Reichardt's polarity parameter. Error bars represent the estimated measurement uncertainty.

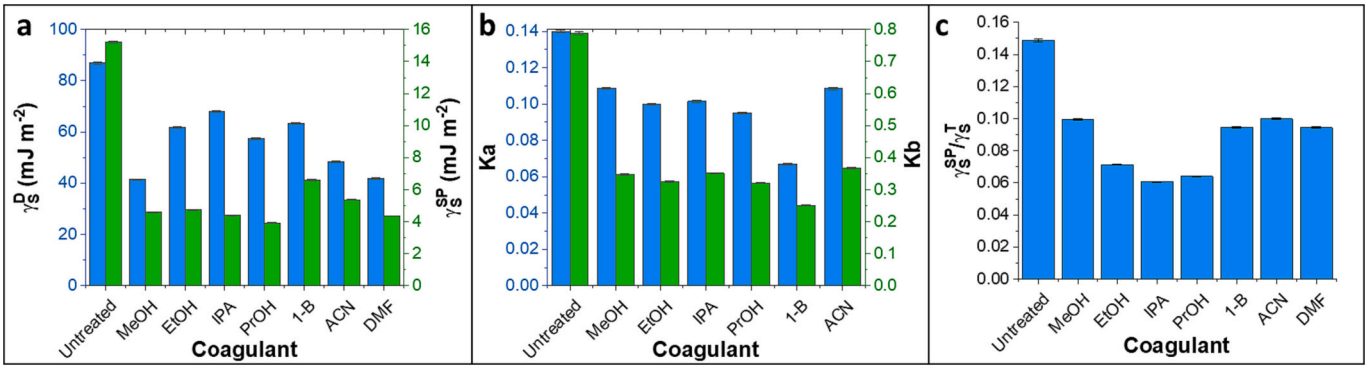

Fig. 4. Comparison of (a) dispersive surface area (left y-axis, blue) and specific surface area (right y-axis, green), (b) Lewis acid constant (left y-axis, blue) and Lewis base constant (right y-axis, green), and (c) hydrophilicity at 5 % surface coverage in regenerated cellulose fabricated using different coagulation solvents. Coagulation solvents are listed in order of decreasing solvent polarity from left to right using the normalized Reichardt's polarity parameter. Error bars represent the estimated measurement uncertainty.

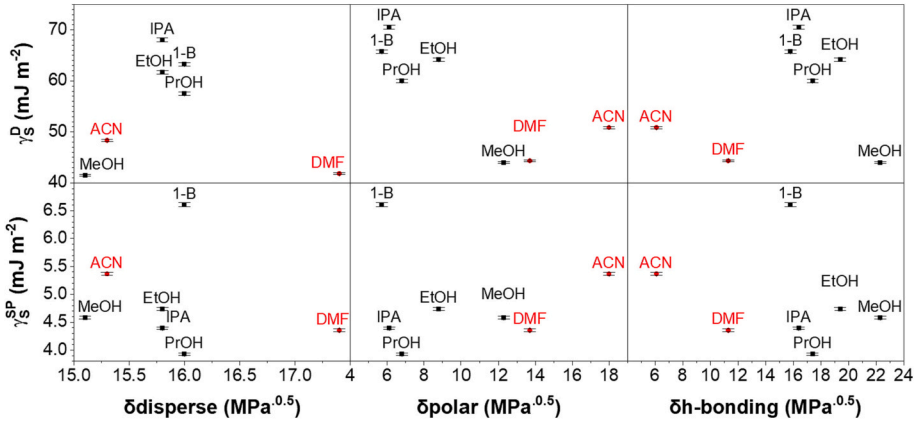

Fig. 5. Comparison of dispersive surface energy (γ_S^D, top panel) and specific surface energy (γ_S^{SP}, bottom panel) measured using iGC 5 % surface coverage of samples fabricated using different protic (black circles) and aprotic (red squares) coagulation solvents with Hansen-solubility parameters of the coagulation solvent. Error bars represent the estimated measurement uncertainty.

the exception of DMF ($\delta_{disperse} = 17.4$). No observable correlation was found relating to hydrogen bond strength. Again, additional solvent studies are required to more clearly define the role of solubility on surface hydrophilicity.

Although hydrophilicity is dictated by surface energy, a comparison of K_a and K_b with the Hansen solubility parameters of the coagulation

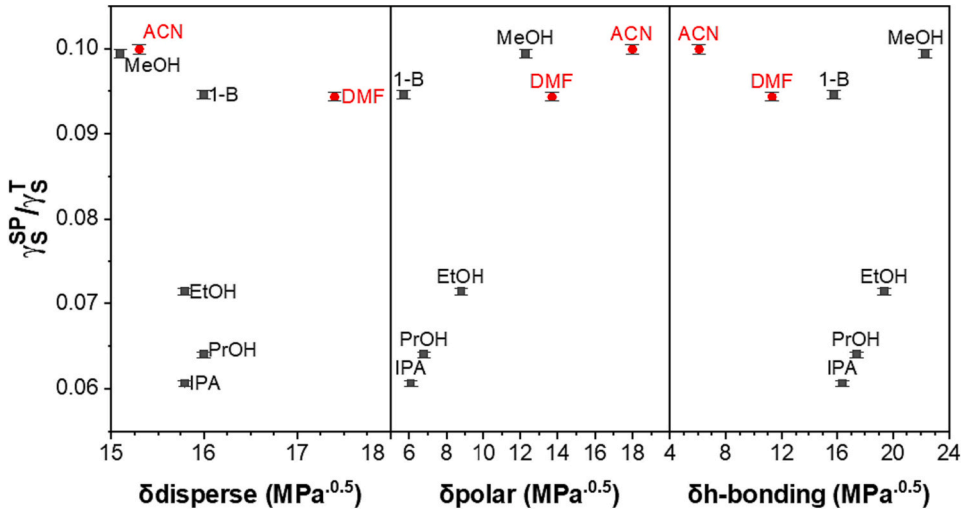

Fig. 6. Comparison of hydrophilicity at 5 % surface coverage of samples fabricated using different protic (black squares) and aprotic (red circles) coagulation solvents with Hansen-solubility parameters of the coagulation solvent. Error bars represent the estimated measurement uncertainty.

solvents are also provided (Fig. S2). Both K_a and K_b show the same general behavior for changes in the Hansen solubility parameters where the constant decreases with increasing $\delta_{disperse}$, increases with increasing δ_{polar}, and is independent of $\delta_{h\text{-}bonding}$.

4. Discussion

Cellulose is an amphiphilic linear polymer with both hydrophilic (hydroxyl groups at the surface in the $(1\bar{1}0)$ crystal plane) and hydrophobic (aliphatic groups at the surface in the (110) plane) orientations (Yamane et al., 2006). Fig. 7 compares the surface hydrophilicity with specific surface area. This comparison shows a clearly defined relationship where the BET surface area decreases significantly from 100 m^2 g^{-1} to 0.278 m^2 g^{-1} with increasing hydrophilicity, indicating that controlling the hydrophobic orientation in regenerated cellulose plays an important role in controlling the porosity of cellulose xerogels, although this is also applicable to cellulose cryo- and aerogels. Increasing the hydrophobicity of the surface may also improve the robustness of the porous matrix by reducing swelling in the presence of atmospheric water.

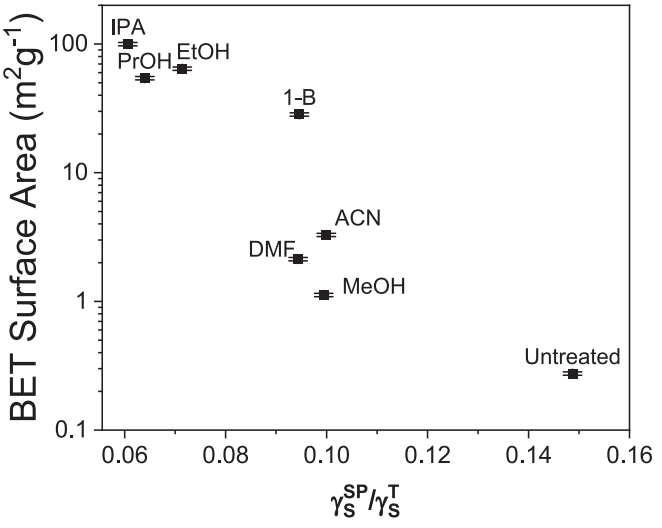

Fig. 7. Comparison of specific surface area with surface hydrophilicity (5 % surface coverage) for samples fabricated using different coagulation solvents. Error bars represent the estimated measurement uncertainty.

The combined iGC, BET, and XPS results suggest that while the coagulation solvent plays a strong role in the regenerated cellulose orientation, cellulose dissolved in $[C_2C_1Im][OAc]$ prefers to regenerate in the hydrophilic orientation. Previous studies have attributed the use of fluids with surface tensions lower than that of water (i.e., < 0.073 N m^{-1}) to porous network formation in xerogels, as this can minimize hornification effects (Budtova, 2019). Our measurements do not support this hypothesis. As seen in Fig. S3, surface tension showed no effect on specific surface area. While decreasing solvent polarity does produce a more hydrophobic regenerated cellulose surface, it also decreases the IL and water solvation effectiveness. This plays an important role in the kinetics of cellulose regeneration where regeneration is slowed as the IL and water solvation ability decreases. For sufficiently slowed cellulose regeneration rates, the dissolved cellulose chains are provided more time to shift from the initial hydrophobic orientation induced by the hydrophobic solvent to a more thermodynamically favorable hydrophilic orientation (Fig. 4c). Our results suggest that maximizing the polar interaction strength and/or minimizing the coagulation solvent dispersion force strength is one way to maximize the hydrophobic orientation of the regenerated cellulose surface and subsequently maximize the specific surface area of cellulose xerogels. Similar kinetic effects have been reported in studies of regenerated cellulose crystallinity from aqueous solutions using different coagulation baths (From et al., 2020). This effect is likely due to reorganizational effects produced by phase separation of different components in the coagulation bath, which are driven by the solubility characteristics of the coagulation solvent. However, further experimentation is required to elucidate the role of competing kinetics and thermodynamics in this system.

Finally, we propose the following pore formation mechanism, as illustrated in Fig. 8, which combines the results presented in this paper with our recent findings regarding room temperature crystallization of $[C_2C_1Im][OAc]$ (Aiello, Hoffman, Flagg, & Woodcock, 2023). Specifically, we have recently observed room temperature crystallization of $[C_2C_1Im][OAc]$ upon removal of trace water from the system using 2D wide-angle X-ray scattering, Raman, and simultaneous quartz crystal microbalance/infrared spectroscopy measurements. This experimentally shows that even trace water dramatically impacts molecular organization of the IL. This presents the possibility that strongly organized, or even crystallized (e.g. liquid or solid crystals), $[C_2C_1Im][OAc]$ may serve as a template for porous morphology evolution during coagulation, especially in phase-separated IL regions. For this to occur, the coagulation solvent must interact more strongly with water compared with the IL to preferentially remove water from the IL. As trace water is removed from the IL, crystallization of the IL can occur. This is a

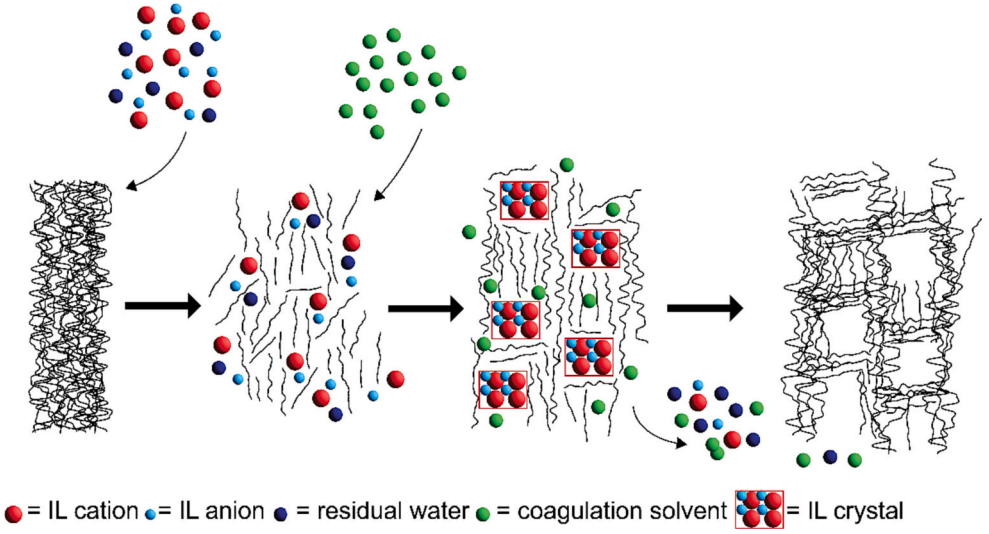

Fig. 8. Cartoon of the proposed pore formation mechanism. First, IL containing trace amounts of water is introduced to the cellulose yarn to dissolve cellulose chains. Next, a coagulation solvent is introduced to remove IL from the system and regenerate the dissolved cellulose. Coagulation solvents that form stronger interactions with water than the IL can preferentially remove water from the system, allowing for crystalline IL formation. These crystals serve as a template for the dissolved cellulose chains to regenerate around. As the coagulation solvent continues to remove IL, a porous matrix is left behind.

kinetically driven process where the crystal size and structure would be governed by time dynamics. These crystals may then serve as a template for the dissolved cellulose chains to regenerate around, leaving a porous matrix behind as the coagulation solvent eventually removes the residual IL. Viscometric studies have shown that small additions of water (e.g., trace water) increase cellulose solubility in [C_2C_1Im][OAc] (Le, Sescousse, & Budtova, 2011). Additionally, trace water in [C_2C_1Im][OAc] has been shown to form ordered structures (Hall et al., 2012), which may play a role in the formation of lyotropic liquid crystalline solutions and liquid crystalline gels in cellulose-[C_2C_1Im][OAc] solutions (Song, Niu, Wang, & Zhang, 2011). As such, it is plausible that removal of trace water from the system would decrease cellulose solubility and facilitate the formation of cellulose aggregates around IL crystals, which would also influence the preferred orientation. Once formed, cellulose gels have been shown to be robust, even during cyclic heating and cooling events (Cai & Zhang, 2006). This may also account for the consistency in pore size despite the use of various coagulation solvents where pore size is controlled by the IL used to dissolve the cellulose chains. Thus, tunable pore size may be achievable with the use of different ILs for cellulose dissolution. Although this working hypothesis requires additional study in the form of future in-situ small- and wide-angle X-ray scattering experiments, the formation of ordered structures, including liquid crystalline gels, has already been reported in concentrated microcrystalline cellulose-[C_2mim][OAc] solutions exceeding 12.5 % mass fraction (Song et al., 2011).

5. Conclusion

The impact of coagulation solvent interactions during cellulose xerogel fabrication was evaluated by comparing seven different coagulation baths with varying solvent polarity (i.e., MeOH, EtOH, IPA, PrOH, 1-B, ACN, and DMF) using cotton yarns partially dissolved in [C_2C_1Im][OAc]. The regenerated cellulose xerogels were found to be more homogenous than undissolved cellulose Iβ with respect to dispersive surface energy, specific surface energy, Lewis acid constant, Lewis base constant, and hydrophilicity. Additionally, these surface properties were impacted by the coagulation solvent polarity where the dispersive surface energy was maximized and the Lewis acid constant and hydrophilicity were minimized for mid-range solvent polarity ($0.52 < E_N^T < 0.55$). The Hansen solubility parameters of the coagulation solvents were compared to assess the role of dispersion force strength, polar interaction strength, and hydrogen bond strength. The polar interaction strength showed the strongest overall relationship with the measured surface properties, followed by the dispersion force strength. Hydrogen bond strength did not play a strong role in the measured surface energy and hydrophilicity. The specific surface area showed a strong relationship with hydrophilicity where the xerogel specific surface area decreased from 100 $m^2\ g^{-1}$ to 0.278 $m^2\ g^{-1}$ with a relatively small increase in hydrophilicity from 0.06 to 0.15. These results were attributed to polarity-driven interactions between the IL, trace water, cellulose, and the coagulation solvent as well as the IL and water solvation ability of the coagulation solvent, which result in competing thermodynamic and kinetic interactions. We have used these findings to propose a pore formation mechanism where a porous matrix is produced by preferential water solvation by the coagulation solvent to remove trace water from the coagulation bath, allowing for IL crystallization for pore templating. Identification of the pore formation mechanism is crucial for the development of both tunable porosity and compatible functionalization reactions needed for advanced cellulose xerogel applications including separations and membranes. Even more importantly, this processing technique is compatible with commercially produced cotton textiles and may be a viable way to reduce textile waste as part of new circular economy applications.

CRediT authorship contribution statement

Ashlee Aiello: Conceptualization, Investigation and Methodology (sample fabrication, iGC), Writing – Original Draft, Review, and Editing, Visualization, **Huong Giang Nguyen:** Investigation and Methodology (N_2 physisorption), **Christopher M. Stafford:** Investigation and Methodology (XPS), **Jeremiah W. Woodcock:** Supervision, Conceptualization, Methodology (sample fabrication, iGC), Writing—Review and Editing.

Declaration of competing interest

The authors declare that they have no known competing financial interests or personal relationships that could have appeared to influence the work reported in this paper.

Data availability

No data was used for the research described in the article.

Acknowledgements

A.A. acknowledges financial support from the National Research Council through the Research Associateship Program. Official contribution of the National Institute of Standards and Technology; not subject to copyright in the United States.

Appendix A. Supplementary data

Supplementary data to this article can be found online at https://doi.org/10.1016/j.carbpol.2023.121454.

References

Aiello, A., Cosby, T., Durkin, D. P., & Trulove, P. C. (2022). Macroscale time-dependent ionic liquid treatment effects on biphasic cellulose xerogels. *Cellulose, 29*(16), 8695–8704.

Aiello, A., Cosby, T., McFarland, J., Durkin, D. P., & Trulove, P. C. (2022). Mesoporous xerogel cellulose composites from biorenewable natural cotton fibers. *Carbohydrate Polymers, 282*, 119040.

Aiello, A., Hoffman, J., Flagg, L., & Woodcock, J. (2023). Trace water effects on crystalline 1-ethyl-3-methylimidazolium acetate. *Journal of Physical Chemistry B, 127*(20), 4595–4601.

Al-Ghouti, M. A., & Da'ana, D. A. (2020). Guidelines for the use and interpretation of adsorption isotherm models: A review. *Journal of Hazardous Materials, 393*, 122383.

Alves, L., Medronho, B. F., Antunes, F. E., Romano, A., Miguel, M. G., & Lindman, B. (2015). On the role of hydrophobic interactions in cellulose dissolution and regeneration: Colloidal aggregates and molecular solutions. *Colloids and Surfaces A: Physicochemical and Engineering Aspects, 483*, 257–263.

Bosch, E., & Roses, M. (1992). Relationships between E_T polarity and composition in binary solvent mixtures. *Journal of the Chemical Society, Faraday Transactions, 24*(88), 3541–3546.

Buchtová, N., & Budtova, T. (2016). Cellulose aero-, cryo- and xerogels: Towards understanding of morphology control. *Cellulose, 23*(4), 2585–2595.

Budtova, T. (2019). Cellulose II aerogels: A review. *Cellulose, 26*(1), 81–121.

Budtova, T., & Navard, P. (2015). Cellulose in NaOH–water based solvents: A review. *Cellulose, 23*(1), 5–55.

Cai, J., & Zhang, L. (2006). Unique gelation behavior of cellulose in NaOH/urea aqueous solution. *Biomacromolecules, 7*, 183–189.

Dutkiewicz, M. (1990). Classification of organic solvents based on correlation between dielectric β parameter and empirical solvent polarity parameter E^{NT}. *Journal of the Chemical Society, Faraday Transactions, 86*(12), 2237–2241.

From, M., Larsson, P. T., Andreasson, B., Medronho, B., Svanedal, I., Edlund, H., & Norgren, M. (2020). Tuning the properties of regenerated cellulose: Effects of polarity and water solubility of the coagulation medium. *Carbohydrate Polymers, 236*, 116068.

Gamelas, J. A. F. (2013). The surface properties of cellulose and lignocellulosic materials assessed by inverse gas chromatography: A review. *Cellulose, 20*(6), 2675–2693.

Ganesan, K., Dennstedt, A., Barowski, A., & Ratke, L. (2016). Design of aerogels, cryogels and xerogels of cellulose with hierarchical porous structures. *Materials & Design, 92*, 345–355.

Geng, X., & Henderson, W. A. (2014). Impact of non-solvents on the structural features and enzymatic digestibility of cellulose regenerated from an ionic liquid. *RSC Advances, 4*(59), 31226–31229.

Gericke, M., Schlufter, K., Liebert, T., Heinze, T., & Budtova, T. (2009). Rheological properties of cellulose/ionic liquid solutions: From dilute to concentrated states. *Biomacromolecules, 10*, 1188–1194.

Hall, C. A., Le, K. A., Rudaz, C., Radhi, A., Lovell, C. S., Damion, R. A., … Ries, M. E. (2012). Macroscopic and microscopic study of 1-ethyl-3-methyl-imidazolium acetate-water mixtures. *The Journal of Physical Chemistry. B, 116*(42), 12810–12818.

Jessop, P. G., Jessop, D. A., Fu, D., & Phan, L. (2012). Solvatochromic parameters for solvents of interest in green chemistry. *Green Chemistry, 14*(5).

Jin, H., Nishiyama, Y., Wada, M., & Kuga, S. (2004). Nanofibrillar cellulose aerogels. *Colloids and Surfaces A: Physicochemical and Engineering Aspects, 240*(1–3), 63–67.

Le, K. A., Sescousse, R., & Budtova, T. (2011). Influence of water on cellulose-EMIMAc solution properties: A viscometric study. *Cellulose, 19*(1), 45–54.

Lindman, B., Karlström, G., & Stigsson, L. (2010). On the mechanism of dissolution of cellulose. *Journal of Molecular Liquids, 156*(1), 76–81.

Medronho, B., Duarte, H., Alves, L., Antunes, F. E., Romano, A., & Lindman, B. (2015). Probing cellulose amphiphilicity. *Nordic Pulp & Paper Research, 30*(1), 58–66.

Medronho, B., & Lindman, B. (2014). Competing forces during cellulose dissolution: From solvents to mechanisms. *Current Opinion in Colloid & Interface Science, 19*(1), 32–40.

Medronho, B., & Lindman, B. (2015). Brief overview on cellulose dissolution/regeneration interactions and mechanisms. *Advances in Colloid and Interface Science, 222*, 502–508.

Medronho, B., Romano, A., Miguel, M. G., Stigsson, L., & Lindman, B. (2012). Rationalizing cellulose (in)solubility: Reviewing basic physicochemical aspects and role of hydrophobic interactions. *Cellulose, 19*(3), 581–587.

Mohammadi-Jam, S., & Waters, K. E. (2014). Inverse gas chromatography applications: A review. *Advances in Colloid and Interface Science, 212*, 21–44.

Östlund, Å., Idström, A., Olsson, C., Larsson, P. T., & Nordstierna, L. (2013). Modification of crystallinity and pore size distribution in coagulated cellulose films. *Cellulose, 20*(4), 1657–1667.

Ramamoorthy, S. K., Skrifvars, M., & Persson, A. (2015). A review of natural fibers used in biocomposites: Plant, animal and regenerated cellulose fibers. *Polymer Reviews, 55*(1), 107–162.

Reichardt, C. (1994). Solvatochromic dyes as solvent polarity indicators. *Chemical Reviews, 94*, 2319–2358.

Reichardt, C. (2005). Polarity of ionic liquids determined empirically by means of solvatochromic pyridinium N-phenolate betaine dyes. *Green Chemistry, 7*(5).

Sing, K. S. W., Everett, D. H., Rierotti, R. A., Rouquerol, J., & Siemieniewska, T. (1985). Reporting physisorption data for gas/solid systems with special reference to the determination of surface area and porosity. *Pure and Applied Chemistry, 57*(4), 603–619.

Sing, K. S. W., & Williams, R. T. (2004). Physisorption hysteresis loops and the characterization of nanoporous materials. *Adsorption Science and Technology, 22*(10), 773–782.

Song, H., Niu, Y., Wang, Z., & Zhang, J. (2011). Liquid crystalline phase and gel-sol transitions for concentrated microcrystalline cellulose (MCC)/1-ethyl-3-methylimidazolium acetate (EMIMAc) solutions. *Biomacromolecules, 12*(4), 1087–1096.

Yamane, C., Aoyagi, T., Ago, M., Sato, K., Okajima, K., & Takahashi, T. (2006). Two different surface properties of regenerated cellulose due to structural anisotropy. *Polymer Journal, 38*(8), 819–826.

Yamasaki, S., Sakuma, W., Yasui, H., Daicho, K., Saito, T., Fujisawa, S., … Kanamori, K. (2019). Nanocellulose xerogels with high porosities and large specific surface areas. *Frontiers in Chemistry, 7*.